Carbon 111 (2017) 529–537

Contents lists available at ScienceDirect

Carbon

journal homepage: www.elsevier.com/locate/carbon

Carbon nanofiber mats for electromagnetic interference shielding

Xinghua Hong [a, b], D.D.L. Chung [a, *]

[a] Composite Materials Research Laboratory, Department of Mechanical and Aerospace Engineering, University at Buffalo, The State University of New York, Buffalo, NY, 14260-4400, USA
[b] Key Laboratory of Textile Science & Technology, Ministry of Education, College of Textiles, Donghua University, Shanghai, 201620, China

ARTICLE INFO

Article history:
Received 13 September 2016
Received in revised form
13 October 2016
Accepted 14 October 2016
Available online 14 October 2016

ABSTRACT

This paper reports the electromagnetic interference shielding effectiveness of carbon nanofiber (CNF, originally called carbon filament) mats made from 0.16-μm-diameter catalytically grown CNFs by the paper-making process (1.7–13.1 MPa compaction pressure). These low-cost lightweight binderless mats (2.9–5.4 mm thick, 0.13–0.22 g/cm^3 bulk density, 6.1–10 vol% solid) provide high shielding effectiveness (*SE*, 52–81 dB, 1.5 GHz) and high *SE*/density (370–470 dB cm^3/g), though *SE*/thickness is low (14–18 dB/mm). Compared to the spun CNF mats of prior work, they exhibit higher *SE*, but lower *SE*/thickness. With consideration of *SE*, *SE*/thickness, and *SE*/density, the CNF mats are superior to graphene aerogel, reduced-graphene-oxide polyurethane foam and reduced-graphene-oxide aerogel of prior work, but are inferior to carbon nanotube mats, graphene film, carbon foam and flexible graphite of prior work. Absorption is the dominant shielding mechanism of CNF mats, so both *SE* and absorption loss tend to decrease with decreasing thickness. The absorption-loss/thickness tends to decrease with increasing thickness. The reflection loss is independent of the thickness, density or mass, indicating saturated reflection. The reflection-loss/density increases with decreasing density, suggesting that a higher degree of three-dimensional electrical connectivity, as provided by a lower density, enables the reflection to occur at a greater depth into the mat surface.

1. Introduction

Electromagnetic interference (EMI) shielding is needed for the protection of electronics from radio waves and for the shielding of radiation sources. In addition, it is relevant to radars, wireless communication and electrostatic discharge protection. Furthermore, a high shielding effectiveness alleviates the problem of electronic pollution emanating from radio frequency wireless communication devices and other electronic equipment.

1.1. Shielding materials comprising carbon

Carbon materials are attractive for EMI shielding due to their ability to absorb and reflect electromagnetic radiation. Table 1 lists the competing top-performance carbon –containing shielding materials of prior work [1–15]. The attributes listed include the shielding effectiveness, the shielding effectiveness per unit thickness and the shielding effectiveness per unit density. Because the shielding material is in the form of a sheet, and because of the linear increase of the absorption loss in dB with increasing thickness, the shielding effectiveness per unit thickness is an important attribute. For aerospace and other weight-sensitive applications, lightweight materials for EMI shielding are needed. Thus, the shielding effectiveness per unit density (known as the specific shielding effectiveness) is another useful attribute. High values are desirable for all three attributes – shielding effectiveness, shielding effectiveness per unit thickness and shielding effectiveness per unit density.

Among the materials listed in Table 1, flexible graphite (compacted exfoliated graphite) gives the highest value of the shielding effectiveness (102–129 dB) [1]. On the other hand, in relation to the shielding effectiveness per unit thickness, carbon nanotube (CNT) mat with iron nanoparticles gives the highest value of 40,000 dB/mm [11], CNT mat without iron nanoparticles gives the second highest value of 30,000 dB/mm [11], and graphene film gives the third highest value of 4160 dB/mm [3]. Although flexible graphite gives lower values of the shielding effectiveness per unit thickness than CNT mats, graphene films or carbon foam, it gives much higher

* Corresponding author.
E-mail address: ddlchung@buffalo.edu (D.D.L. Chung).
URL: http://alum.mit.edu/www/ddlchung

http://dx.doi.org/10.1016/j.carbon.2016.10.031
0008-6223/

Table 1
EMI shielding effectiveness of competing carbon-containing materials. RGO = reduced graphene oxide. GNP = graphite nanoplatelet. CF = carbon fiber. NF = nanofiber. The density refers to the bulk density.

Material	Shielding effectiveness (dB)	Shielding effectiveness per unit thickness (dB/mm)	Shielding effectiveness per unit density (dB cm^3/g)	Ref.
Flexible graphite	102	129	93	[1]
Flexible graphite	129	42	118	[1]
Carbon foam	24	1000	/	[2]
Graphene film	32	4160	/	[3]
Graphene film	65	1300	/	[4]
Graphene aerogel	37	12	530	[5]
Graphene foam	25	84	420	[6]
RGO aerogel	24	2	1440	[7]
Graphene/PDMS foam	30	30	500	[8]
RGO/PU foam	20	/	253	[9]
RGO/SiO_2	38	25	/	[16]
GNP polymer composite	70	88	67	[10]
CNT mat	30	30,000	/	[11]
Fe/CNT mat	40	40,000	/	[11]
CNF mat	38	190	/	[12]
CNF mat	44	63	/	[13]
CNF mat	81	18	370	This work
CNF mat	75	14	470	This work
CNF mat	52	18	390	This work
Fe_3O_4/CNF mat	68	97	/	[13]
Cu/PVA NF mat	32	1600	/	[14]
CF mat	23	380	/	[15]
Ni/CF mat	29	480	/	[15]

shielding effectiveness that ranges from 102 to 129 dB, in contrast to the values ranging from 24 to 65 dB for the CNT mats, graphene films and carbon foam.

With respect to the shielding effectiveness per unit density, reduced graphene oxide (RGO) foam gives the highest value of 1440 dB cm^3/g [7], while graphene foam gives the next highest value of 530 dB cm^3/g [5] and graphene/polydimethylsiloxane (PDMS) foam gives the still next highest value of 500 dB cm^3/g [8]. In spite of the high values of the shielding effectiveness per unit thickness, RGO foam, graphene foam and graphene/PDMS foam exhibit low values (ranging from 24 to 37 dB) of the shielding effectiveness and low values (ranging from 2 to 30 dB/mm) of the shielding effectiveness per unit thickness. The silica-matrix RGO composite [16] is not attractive in comparison to most of the other materials listed in Table 1, though it is advantageous in its ability to withstand elevated temperatures.

For EMI shielding, a small diameter is preferred for the conductive fibers because of the skin effect. Due to the skin effect, fibers of a smaller diameter is more effective for shielding than those of a larger diameter for the same fiber composition and the same fiber volume fraction. Therefore, carbon nanofiber (CNF, originally known as carbon filament) and CNT are more effective than short carbon fibers [17].

A 0.2-mm thick CNF mat made of 190-nm diameter CNFs that are prepared by 800°C-carbonization of centrifugal-force spun polyvinyl alcohol (PVA) fibers exhibits in-plane electrical resistivity 0.41 Ω cm and EMI shielding effectiveness 38 dB at 1 GHz [12]. A CNF mat with 5 wt% Fe_3O_4 (44 nm particles) incorporated in each CNF gives a mat (0.7 mm thick) with shielding effectiveness 68 dB at 8 GHz [13]. Without the Fe_3O_4 particles, the shielding effectiveness is lower - 44 dB at 8 GHz [13]. The use of CNF (0.16 μm diameter, specific surface area 12.5 m^2/g, 19 vol%) as a filler in polyether sulfone gives a composite that exhibits shielding effectiveness 74 dB at 1–2 GHz and DC electrical resistivity 0.1 Ω cm [18]. The use of CNF (0.1–0.2 μm diameter, 30–100 μm long, 20 wt%) as a filler in polystyrene gives a composite that exhibits shielding effectiveness 35 dB at 12.4 GHz [19]. A mat (60 μm thick) consisting of nickel-coated carbon fibers (7 μm diameter, 6 mm long) exhibits shielding effectiveness 29 dB at 1 GHz [15].

1.2. Carbon mats

Discontinuous fibers, nanofibers or nanotubes are commonly used in the form of mats. A mat consists of a number of discontinuous fibrous units that are not woven, but are weakly held together by van der Waals forces. The fibrous units are typically not aligned. There is no matrix material, so that a mat includes a high volume fraction of air voids. A small amount of binder is optionally used to help bind the fibers together at their junctions. Mats are commonly made by using a paper-making process, which involves the dispersion of the fibers in a liquid medium, followed by casting and drying. The liquid medium commonly includes a minor amount of a binder, such as polytetrafluoroethylene (PTFE) and a phenolic resin [20]. The organic binder such as phenolic may be subsequently carbonized by heating. Another method involves the pressing and subsequent carbonization of a carbon fiber felt that has been impregnated with a carbon precursor, such as a phenolic resin [21]. A related method involves using a mixture of carbon fibers and polyacrylonitrile (PAN) fibers to form a mat by wet laying, followed by the carbonization of the PAN fibers, which act as a binder [22,23]. After the carbonization, the mat is a carbon-carbon composite that is highly porous. Yet another method involves spinning a polymer-based precursor to form a polymer-based nanofiber mat upon deposition, followed by carbonization [12,13]. Surface treatment of the fibers (e.g., oxidation, plasma and chemical treatments) can be used to improve the dispersion [24] and adhesion [25] of the fibers. The fabrication of mats is simpler than that of the RGO foam [7], graphene foam [5], graphene PDMS foam [8] and carbon foam [2].

The CNF mats have been previously reported in terms of the electrical resistivity and conduction applications [26,27], in addition to EMI shielding mentioned above [11–14]. Mats made with CNFs of different diameters show that the mat resistivity is lower for the larger CNF diameter. This is because of the larger number of CNF-CNF contacts per unit volume of the mat when the CNF diameter is small. Each contact is associated with electrical resistance. Furthermore, a larger CNF diameter tends to cause the CNF-CNF contact area to be larger, hence decreasing the resistance of the contact. On the other hand, graphitization of the CNF results in a

reduction in the resistivity of the CNF mat. However, coating the CNF with nickel by electroplating results in an even greater reduction of the resistivity of the mat [26].

The use of a CNF mat in place of carbon black as porous reduction electrodes (i.e., current collectors) in carbon limited lithium batteries with the BCX (bromine chloride in thionyl chloride) catholyte gives a specific capacity (at 2 V cut-off) of up to 8700 mA h/g of carbon, compared with a value of up to 2900 mA h/g of carbon for carbon black. The high specific capacity for the CNF electrode is partly due to the CNFs' processability into sheets as thin as 0.2 mm with good porosity, acceptable mechanical properties and without binder, and partly due to the high catholyte absorptivity and high rate of catholyte absorption of the CNF electrode [27].

Three-dimensional mats of entangled CNFs have been fabricated by thermal chemical vapor deposition, involving the use of an unconstrained Ni-Pd film (not bound to a substrate) as the catalyst. The mats are potentially attractive for use as the anode of a lithium-ion battery [28].

Carbon nanotube (CNT) mats have been reported for various electrical conduction and dielectric applications, in addition to EMI shielding mentioned above [11]. A CNT mat of thickness 65 μm, density 0.25 g/cm^3 and porosity 86%, as made by compacting MWCNTs of length 1 mm, exhibits electrical resistivity 6.5×10^{-3} Ω cm [29]. Single-walled semiconducting CNT mats in the form of flexible thin films are attractive for electronic and photonic devices. They are amenable to large-area thin-film manufacturing and patterning. Applications include field-effect transistors, sensors, detectors, photovoltaic cells and light emitting diodes [30].

1.3. Mats for EMI shielding

Prior work on the effectiveness of mats for EMI shielding is reviewed below. A mat (60 μm thick) of carbon fibers (not nanofibers, 10 μm diameter, 6–13 mm long) exhibits shielding effectiveness 23 dB at 1 GHz [15]. With nickel coating (50 wt% Ni or 20 vol% Ni for the coated fiber, corresponding to a radius increase of 13% due to the coating) on the carbon fibers (6 mm long), the shielding effectiveness of the mat (60 μm thick) is increased to 29 dB [15]. A mat of thickness 1.0 μm, as prepared by the deposition of catalytically grown CNTs, gives shielding effectiveness 30 dB at 1 GHz [11], i.e., shielding effectiveness per unit thickness 30,000 dB/mm. If extra iron particles are added to the mat, the shielding effectiveness is increased to 40 dB at 1 GHz [11], i.e., shielding effectiveness per unit thickness 40,000 dB/mm. A mat of thickness 0.5 mm and consisting of electrospun polyaniline nanofibers and gold nanoparticles, gives shielding effectiveness up to 23 dB (11.2 GHz) [31]. An MWCNT-coated Nylon-6 nanofiber mat provides EMI shielding effectiveness 25 dB at 1 GHz [32]. A MWCNT (25%) PMMA-matrix composite nanofiber of diameter 370–800 nm is used to form a mat, which exhibits EMI shielding effectiveness 30 dB at 1 GHz [33]. An electrospun MWCNT PVA-matrix composite nanofiber is potentially attractive for EMI shielding, particularly if it is coated with copper [34]. A magnetic filler (5 wt% Fe_3O_4) is incorporated in CNF by electrospinning of a PAN-based precursor, followed by carbonization. The resulting composite nanofiber has diameter 320 nm and provides a mat of thickness 0.7 mm, with shielding effectiveness 68 dB at 8 GHz [13]. Without the magnetic filler, the shielding effectiveness of the CNF mat of the same thickness is 44 dB at 8 GHz [13]. Metal-coated electrospun PVA nanofiber is used to form a mat (~20 μm thick, with the metal being copper of thickness 200 nm), which gives shielding effectiveness 32 dB at 1 GHz [14], i.e., shielding effectiveness per unit thickness 1600 dB/mm. Mats of polypyrrole-coated PAN fibers exhibit a low degree of shielding effectiveness [35]. A 300-μm thick mat of electrospun fibers in the form of CNF (1 wt%, 150 nm diameter) filled poly(ε-caprolactone) exhibits reflection loss 14.5 dB at 8 GHz [36]. In a prior work [37], carbon fiber fabric was studied, though the material was referred to as a mat.

In spite of the prior work mentioned above and in Table 1, there is little prior work on the processing-structure-property relationships of materials for EMI shielding. Structural parameters include the density, solid volume fraction, thickness, mass, preferred orientation, electrical connectivity, etc.

The absorption loss in dB by definition is proportional to the thickness, if the linear absorption coefficient is independent of the thickness. However, it may depart from the proportionality because the microstructure of the material (e.g., the degree of preferred orientation of the fibers in the mat) may vary with the thickness, in addition to varying along the thickness direction. Obviously, the microstructure can affect the linear absorption coefficient. For example, in case of mats fabricated in a process that includes compaction, it is likely that the degree of preferred orientation and local density are higher at the two opposite surfaces of the specimen than the interior of the specimen, due to the proximity of these surfaces to the platen surfaces that are providing the compression.

The reflection loss ideally should be independent of the thickness, but it may vary with the thickness because of the penetration of the radiation into the surface and the consequent occurrence of reflection in a region within a certain depth into the surface. This penetration can be significant (beyond the skin depth) when the material is highly porous, as in the case of a mat.

For porous materials such as foams, aerogels and mats, the density and solid volume fraction are important structural parameters. In case of mats, the higher the compaction pressure used in the mat fabrication, the higher are the solid volume fraction and the degree of in-plane preferred orientation of the CNFs in the mat [26]. A higher degree of in-plane orientation is expected to reduce the degree of three-dimensional connectivity of the fibers in the mat. It has been previously reported that the lower is the CNF mat density, the lower is the in-plane electrical conductivity of the mat [26]. The relevant mat properties include the shielding effectiveness, the contributions of the absorption loss and reflection loss to the shielding effectiveness, and the electrical conductivity, which relates to the skin depth.

1.4. Objectives

This work is directed at (i) investigating the effectiveness of CNF mats for EMI shielding, (ii) determining the relationships among processing, structure and electromagnetic absorption/reflection behavior of CNF mats made by using the paper-making process, and (iii) comparing the performance of the CNF mats with that of competing materials of prior work. The comparison in (iii) is needed and constitutes a substantial part of this work, due to the recent rapid growth in research on the subject of materials for EMI shielding.

The CNFs of this work are in contrast to the CNFs in the form of Fe_3O_4-particle carbon-matrix composite nanofibers of prior work [13]. In addition, the CNF mats of this work are prepared by a wet paper-making process, in contrast to the spinning processes used in prior work on CNFs with or without embedded Fe_3O_4 particles [12,13]. There is no prior work on the shielding effectiveness of CNF mats that are made by using the paper-making process, even though this process is most common for the fabrication of mats in general.

2. Experimental methods

2.1. Materials

The CNF was commercially made by Applied Sciences, Inc. (Cedarville, OH, U.S.A.), using methane as the primary source gas and an iron containing catalyst. During the CNF growth, hydrogen sulfide was added to the feedstock in a small amount to increase the CNF yield. The CNF has a fishbone morphology [38]. The nanofibers have not been graphitized and are amorphous, with essentially no graphite 002 peak in the X-ray diffraction pattern [39]. The basic properties of the CNF, as provided by Applied Sciences Inc., are listed in Table 2. The surface area in Table 2 is calculated by assuming that the CNF is a solid cylinder with a density of 2 g/cm^3. In reality, the CNF is a microtube with the inner hole diameter varying from approximately 20 to 75 nm, as shown by transmission electron microscopy (TEM) [39]. Fig. 1 shows the intertwined morphology of the CNFs, the length of which exceeds 100 μm [40]. Such intertwined morphology also exists in the CNF mats and enables a degree of three-dimensional connectivity of the CNFs in the mat. The connectivity occurs in spite of the preferred orientation of the CNFs in the plane of the mat.

The CNF material is the same as the type designated "ADNH (as received)" in prior work [26]. However, the method of mat preparation differs from that of the prior work. In the prior work [26], the CNF mats were prepared by compacting the dry CNFs (without a binder) in a steel mold via a matching steel piston at a controlled pressure ranging from 0.35 to 7.0 MPa, as provided by a hydraulic press.

By increasing the pressure, the bulk density (and thereby the CNF volume fraction) of the mat is increased. The pressure causes a degree of preferred orientation of the CNFs in the plane perpendicular to the pressure direction [26]. However, the CNFs are randomly oriented in this plane. The direction of electrical resistivity measurement is in this plane. For a compaction pressure of 0.35 MPa, the resistivity is 0.38 Ω cm and the bulk density is 0.16 g/cm^3. For a pressure of 7.0 MPa, the resistivity is 0.041 Ω cm and the bulk density is 0.56 g/cm^3 [26]. The higher the pressure, the lower is the resistivity and the higher is the bulk density, as expected. The resistivity values of the CNF mats are higher than the value of 7.5×10^{-4} Ω cm for flexible graphite [1].

In this work, the CNF mats are prepared by using the wet papermaking method. The CNFs are dispersed in water in the absence of a binder, using a blender to form a slurry, followed by casting the slurry into a Teflon-lined steel mold and then applying a controlled uniaxial pressure ranging from 1.7 to 13.3 MPa via a matching steel piston for squeezing out most of the water from the cast slurry and consolidating the material to form a wet cake. The higher is the compaction pressure, the higher is the bulk density (the higher is the solid volume fraction) of the resulting mat. By controlling the mass of material in the mold and the compaction pressure, the thickness and bulk density of the resulting mat are controlled. The mold cavity has the same annular shape and dimensions as the specimens used for EMI effectiveness testing.

Table 2
Basic information on the carbon nanofiber.

Diameter (μm)	0.16
Surface area (m^2/g)	12.5
True density (g/cm^3)	2
Aspect ratio	50–200
Surface chemistry	Nitrogen groups
Sizing	None
SEM morphology	Entwined mass

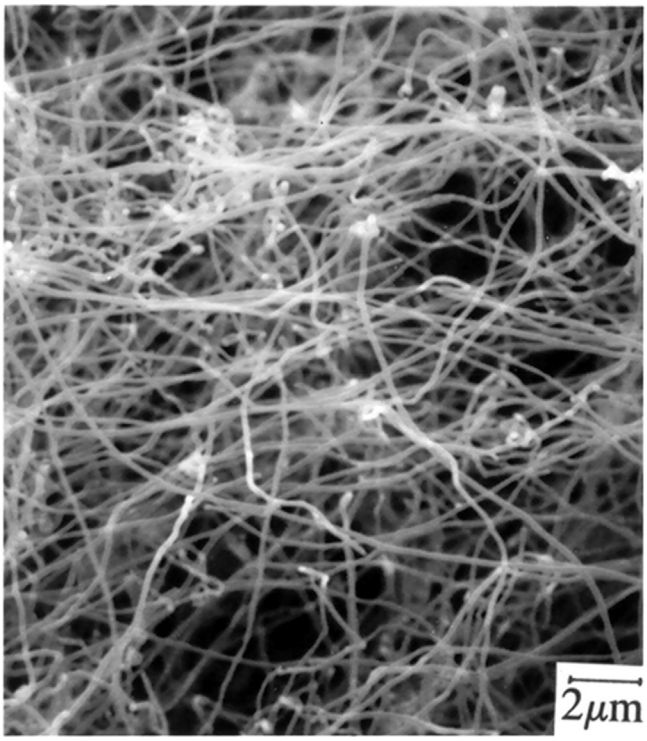

Fig. 1. Scanning electron microscope (SEM) photograph of the carbon nanofibers.

Subsequently, the wet cake is demolded and then dried in air at 105 °C for 6 h in the absence of applied pressure.

2.2. Testing method

The EMI shielding effectiveness is measured by an HP-8510A Network Analyzer using the coaxial cable method. The testing method and equipment are the same as those of prior work [18]. The sample is in the form of an annular ring of outer diameter 98 mm and inner diameter 30 mm. The sample is held by an Elgal SET 19A (Israel) shielding effectiveness tester, which, due to its dimensions, theoretically allows testing at frequencies up to 1.5 GHz. The error in the shielding effectiveness is better than ±1 dB at <10 dB, and ±5 dB at >70 dB. The error increases with increasing attenuation (dB). Prior to the tests, the measurement system is calibrated by using a Hewlett-Packard APC-7 Calibration Kit. The calibration is conducted using the two-ports one-pass method.

2.3. EMI shielding data analysis method

This work addresses the frequency regime in which the electromagnetic radiation propagates mainly by radiation rather than conduction or induction. In general, the electric field in the electromagnetic radiation interacts with the electric dipoles (if any) in the material, while the magnetic field in the radiation interacts with the magnetic dipoles (if any) in the material. In addition, both electric and magnetic fields interact with the mobile electrons (if any) in the material. In this work, no magnetic component is present in the materials.

The loss in electromagnetic radiation propagation is defined as

$$\text{Loss (dB)} = -10 \log(P/P_i), \quad (1)$$

where P is the output power and P_i is the power input. The

logarithm is to the base 10. With $P < P_i$, the loss is positive. The smaller is P, the greater is the loss. Thus, a shielding effectiveness of 40 dB corresponds to an attenuation of 99.99%, for example.

The shielding effectiveness SE_T (total) is given by

$$SE_T = -10 \log(P_t / P_i), \quad (2)$$

where P_t is the transmitted power.

The shielding involves absorption and reflection of the radiation. The part of the shielding due to reflection loss (SE_R) is given by

$$SE_R = -10 \log(1 - R), \quad (3)$$

where R is the fraction of the incident power that is reflected. The part of the shielding due to absorption loss (SE_A) is given by

$$SE_A = -10 \log(T/1 - R), \quad (4)$$

where T is the fraction of the incident power that is transmitted. The absorption loss in dB is proportional to the linear absorption coefficient, which is a material property. The quantities R and T are measured.

3. Results and discussion

As shown in Table 3, a compaction pressure of 6.7 MPa gives a CNF mat with bulk density 0.193 g/cm^3. Prior work [26] on CNF mats fabricated by dry compaction (not the paper-making process) gives a higher bulk density of 0.56 g/cm^3 for a comparable compaction pressure of 7.0 MPa, and requires a lower pressure of 0.70 MPa to obtain a comparable bulk density of 0.20 g/cm^3. The paper-making process results in a lower bulk density for the same pressure, due to the presence of water among the CNFs during the compaction. Although the water completely evaporates during the heating (without pressure) that follows the compaction, the water leaves behind pores, thereby resulting in a lower bulk density for a comparable pressure.

For a similar bulk density, the measured in-plane electrical resistivity is similar between the CNF mat made by the paper-making process of this work and that made by dry compaction in prior work [26]. For Sample 5 (Table 3), the bulk density is 0.159 g/cm^3; this bulk density corresponds to an in-plane resistivity of 0.38 Ω cm [26], which in turn corresponds to a skin depth of 0.80 mm at 1.5 GHz. For Sample 8 (Table 3), the bulk density is 0.193 g/cm^3; this bulk density corresponds to an in-plane resistivity of 0.23 Ω cm [26], which in turn corresponds to a skin depth of 0.62 mm at 1.5 GHz. Samples 8 and 9 are similar in bulk density, so they are similar in the resistivity and skin depth. Samples 6 and 7 have slightly lower bulk density than Sample 5, so their values of the resistivity and skin depth are slightly higher than 0.80 mm at 1.5 GHz. This means that all the samples studied, as listed in Table 3, are thicker than the corresponding skin depth.

Table 3
EMI shielding results of CNT mats. SE_T = shielding effectiveness (total). SE_A = absorption loss. SE_R = reflection loss. The frequency is 1.5 GHz. The columns are in order of decreasing thickness. The density refers to the bulk density.

Sample No.	5	9	8	6	7
Thickness (mm)	**5.426**	**4.634**	**4.385**	**3.524**	**2.862**
Mass (g)	5.763	6.785	5.667	3.757	3.068
Density (g/cm^3)	0.159	0.219	0.193	0.136	0.134
Vol% solid	7.2	10	8.8	6.2	6.1
Compaction pressure (MPa)	3.3	13.3	6.7	1.7	1.7
SE_T (dB)	74.51	81.05	71.21	59.47	52.22
SE_A (dB)	69.20	75.87	65.91	54.15	46.91
SE_R (dB)	5.31	5.18	5.30	5.32	5.31
SE_A/SE	0.93	0.94	0.93	0.91	0.90
SE_R/SE	0.071	0.064	0.074	0.089	0.10
SE_T/thickness (dB/mm)	13.9	17.5	16.2	16.9	18.2
SE_A/thickness (dB/mm)	12.8	16.4	15.0	15.4	16.4
SE_R/thickness (dB/mm)	0.979	1.12	1.21	1.51	1.86
SE_T/density (dB.cm^3/g)	469	370	368	439	391
SE_A/density (dB.cm^3/g)	435	346	342	398	350
SE_R/density (dB.cm^3/g)	33.4	23.7	27.5	39.1	39.6
SE_T/mass (dB/g)	12.9	11.9	12.6	15.8	17.0
SE_A/mass (dB/g)	12.0	11.2	11.6	14.4	15.3
SE_R/mass (dB/g)	0.921	0.763	0.935	1.42	1.73

The shielding results at 1.5 GHz are shown in Table 3. The absorption loss is much higher than the reflection loss, indicating that absorption is the dominant shielding mechanism. Table 3 shows that both the shielding effectiveness and absorption loss tend to decrease with decreasing thickness. This is consistent with the fact that absorption is the dominant shielding mechanism.

Table 3 further shows that, for the range of samples studied, the absorption loss per unit thickness tends to decrease with increasing thickness, although Sample 9 is an exception to this trend, due to its high bulk density (0.219 g/cm^3). At the highest thickness (Sample 5), the absorption loss per unit thickness is exceptionally low (12.8 dB/mm), probably due to the relatively low bulk density (0.159 g/cm^3) of Sample 5. Comparison of Samples 8 and 9 (similar in thickness) shows that a slightly lower bulk density gives a slightly lower absorption loss per unit thickness.

Comparison of Sample 5 with Samples 6 and 7 (with Sample 5 having much larger thickness and slightly higher bulk density than Sample 6 or 7) shows that a large thickness results in a low value of the absorption loss per unit thickness. Comparison of Samples 6 and 7 (similar in bulk density) shows that a larger thickness (Sample 6) gives a lower absorption loss per unit thickness. Comparison of Sample 5 with Samples 8 and 9 (with Sample 5 having larger thickness and lower bulk density than Sample 8 or 9) shows that a large thickness and a low bulk density result in a low value of the absorption loss per unit thickness.

Theoretically, the absorption loss is proportional to the thickness. The finding that the absorption loss per unit thickness tends to decrease with increasing thickness is attributed to the effect of thickness on the microstructure of the mat. A larger thickness is expected to be associated with less preferred orientation of the CNFs, and consequently more three-dimensional connectivity, which provides to a degree the effect of a waveguide and promotes propagation of the radiation, thereby diminishing the absorption.

Table 3 also shows that the reflection loss is essentially independent of the thickness, and that the reflection loss per unit thickness increases with decreasing thickness. These observations are consistent with the notion that reflection mainly occurs in the surface region of the sample, which is considerably thicker than the skin depth. Furthermore, the degree of preferred orientation is expected to be higher at the two opposite surfaces of the specimen than the interior of the specimen. As a consequence, a thin specimen is expected to have a higher average degree of preferred orientation than a thick specimen. The preferred orientation, particularly that in the surface region, promotes reflection of the radiation.

The essential independence of the reflection loss on the thickness (Table 3), bulk density (Table 4) and mass (Table 5) indicates that saturated reflection occurs for all the samples of this work. This is because the amount of carbon material in all the samples is more than being enough for the bulk material to provide saturated reflection. Saturated reflection refers to the maximum reflection that occurs when the sample thickness is infinite. In other words, for a material with a given density, the saturated reflection is the reflection that cannot be exceeded upon increase of the thickness.

Table 4 shows that the reflection loss per unit bulk density increases with decreasing bulk density. Due to the abovementioned

Table 4
EMI shielding results of CNT mats. SE_T = shielding effectiveness (total). SE_A = absorption loss. RL = reflection loss. The frequency is 1.5 GHz. The data are the same as those in Table 3 except that the columns are in order of decreasing density. The density refers to the bulk density.

Density (g/cm^3)	**0.219**	**0.193**	**0.159**	**0.136**	**0.134**
SE_T (dB)	81.05	71.21	74.51	59.47	52.22
SE_A (dB)	75.87	65.91	69.20	54.15	46.91
SE_R (dB)	5.18	5.30	5.31	5.32	5.31
SE_T/density (dB cm^3/g)	370	368	469	439	391
SE_A/density (dB cm^3/g)	346	342	435	398	350
SE_R/density (dB cm^3/g)	23.7	27.5	33.4	39.1	39.6
SE_T/thickness (dB/mm)	17.5	16.2	13.9	16.9	18.2
SE_A/thickness (dB/mm)	16.4	15.0	12.8	15.4	16.4
SE_R/thickness (dB/mm)	1.12	1.21	0.979	1.51	1.86
SE_T/mass (dB/g)	11.9	12.6	12.9	15.8	17.0
SE_A/mass (dB/g)	11.2	11.6	12.0	14.4	15.3
SE_R/mass (dB/g)	0.763	0.935	0.921	1.42	1.73

Table 5
EMI shielding results of CNT mats. SE_T = shielding effectiveness (total). SE_A = absorption loss. SE_R = reflection loss. The frequency is 1.5 GHz. The data are the same as those in Table 3, except that columns are in order of decreasing mass. The density refers to the bulk density.

Mass (g)	**6.785**	**5.763**	**5.667**	**3.757**	**3.068**
SE_T (dB)	81.05	74.51	71.21	59.47	52.22
SE_A (dB)	75.87	69.20	65.91	54.15	46.91
SE_R (dB)	5.18	5.31	5.30	5.32	5.31
SE_T/mass (dB/g)	11.9	12.9	12.6	15.8	17.0
SE_A/mass (dB/g)	11.2	12.0	11.6	14.4	15.3
SE_R/mass (dB/g)	0.763	0.921	0.935	1.42	1.73
SE_T/thickness (dB/mm)	17.5	13.9	16.2	16.9	18.2
SE_A/thickness (dB/mm)	16.4	12.8	15.0	15.4	16.4
SE_R/thickness (dB/mm)	1.12	0.979	1.21	1.51	1.86
SE_T/density (dB cm^3/g)	370	469	368	439	391
SE_A/density (dB cm^3/g)	346	435	342	398	350
SE_R/density (dB cm^3/g)	23.7	33.4	27.5	39.1	39.6

saturated nature of the reflection, it is feasible for the reflection loss per unit bulk density to increase with decreasing bulk density (Table 4 and Fig. 2(b)). This finding suggests that a greater degree of three-dimensional electrical connectivity, as provided by a lower bulk density, promotes the reflectivity from the bulk material. Three-dimensional connectivity facilitates reflection to occur not only at the surface of the mat, but also at a depth (even beyond the skin depth) into the surface.

Table 4 also shows that the fraction of the shielding effectiveness that is due to absorption decreases with decreasing bulk density, while the fraction due to reflection tends to increase with decreasing bulk density. These trends are consistent with the abovementioned trends concerning the absorption loss and reflection loss.

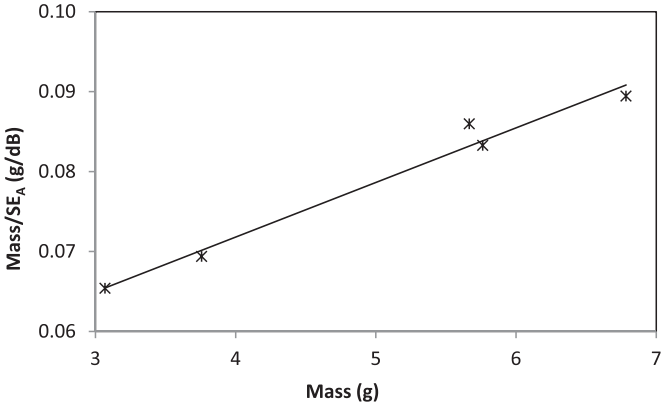

Fig. 2. Plot of mass/SE_A vs. mass. SE_A = absorption loss. The curve is the linear fit.

Table 4 furthermore shows that the shielding effectiveness per unit mass and the absorption loss per unit mass increase with decreasing bulk density, and that the reflection loss per unit mass tends to increase with decreasing bulk density. These trends further support the abovementioned greater efficiency of the CNFs to shield, absorb or reflect when the bulk density of the mat is lower.

Table 5 shows that the shielding effectiveness per unit mass, absorption loss per unit mass and reflection loss per unit mass all increase with decreasing mass. The essential linearity of the plot of the mass/absorption loss vs. mass (Fig. 2) illustrates this trend. This trend means that a smaller amount of CNFs makes the CNFs more efficient in providing both absorption and reflection of the radiation. These findings are attributed to the approximate correlation of low mass and low bulk density, as shown in Table 5. The effect of the bulk density has been discussed above in relation to Table 4.

Fig. 3 shows the linearity of the plots of (a) thickness/SE_R vs. thickness, (b) density/SE_R vs. density, and (c) mass/SE_R vs. mass. The reciprocal of the slopes gives values of SE_R, namely 5.28 dB, 5.06 dB and 5.15 dB for (a), (b) and (c) respectively. These values are close to those in Table 3, thus confirming that the reflection loss is indeed independent of the thickness, bulk density or mass.

Fig. 4 shows that the shielding effectiveness (Fig. 4(a)) and absorption loss (Fig. 4(b)) increase with increasing frequency, whereas the reflection loss (Fig. 4(c)) decreases with increasing frequency. These trends for the absorption loss and reflection loss are expected, based on electromagnetic theory. The shielding is dominated by the absorption loss, with the reflection loss being much lower than the absorption loss. The variation of the reflection loss with the CNF mat formulation (as represented by the Sample No.) is negligible, partly due to the small values of the reflection loss, but the variation is significant for the absorption loss.

Table 1 shows the comparative performance of the CNF mats of this work and carbon-containing materials of prior work. The CNF mats of this work are attractive for providing relatively high values of the shielding effectiveness (52–81 dB) and the shielding effectiveness per unit bulk density (370–470 dB cm^3/g), but they provide relatively low values of the shielding effectiveness per unit thickness (14–18 dB/mm).

Compared to the spun CNF mats of the prior work [12,13], the CNF mats of this work exhibit higher shielding effectiveness. In particular, the shielding effectiveness of some of the CNF mats of this work exceeds the value of 68 dB for the Fe_3O_4-incorporated CNF mat of prior work [13]. However, compared to the spun CNF mats of the prior work [12,13], the CNF mats of this work exhibit lower values of the shielding effectiveness per unit thickness. This is attributed to the larger thickness of the CNF mats of this work (2.9–5.4 mm), compared to the small thickness of 0.2–0.7 mm of the prior work [12,13]. Among the CNF mats in Table 1, the type fabricated by the carbonization of spun PVA fibers [12] gives the lowest shielding effectiveness, but the highest shielding effectiveness per unit thickness. The high shielding effectiveness per unit thickness is probably related to the small thickness (0.2 mm) of this type of mat [12], compared to the larger thickness of 0.7 mm for the type prepared by electrospinning [13] and the still larger thicknesses of the mats in this work. The thickness affects the microstructure through its correlation with the bulk density. In addition, the degree of in-plane preferred orientation of the CNFs is expected to increase with decreasing thickness, due to the geometric constraint in the thickness direction.

The overall performance of the CNF mats is superior to that of graphene aerogel [5] and RGO/PU foam [9], due to the higher shielding effectiveness, higher shielding effectiveness per unit

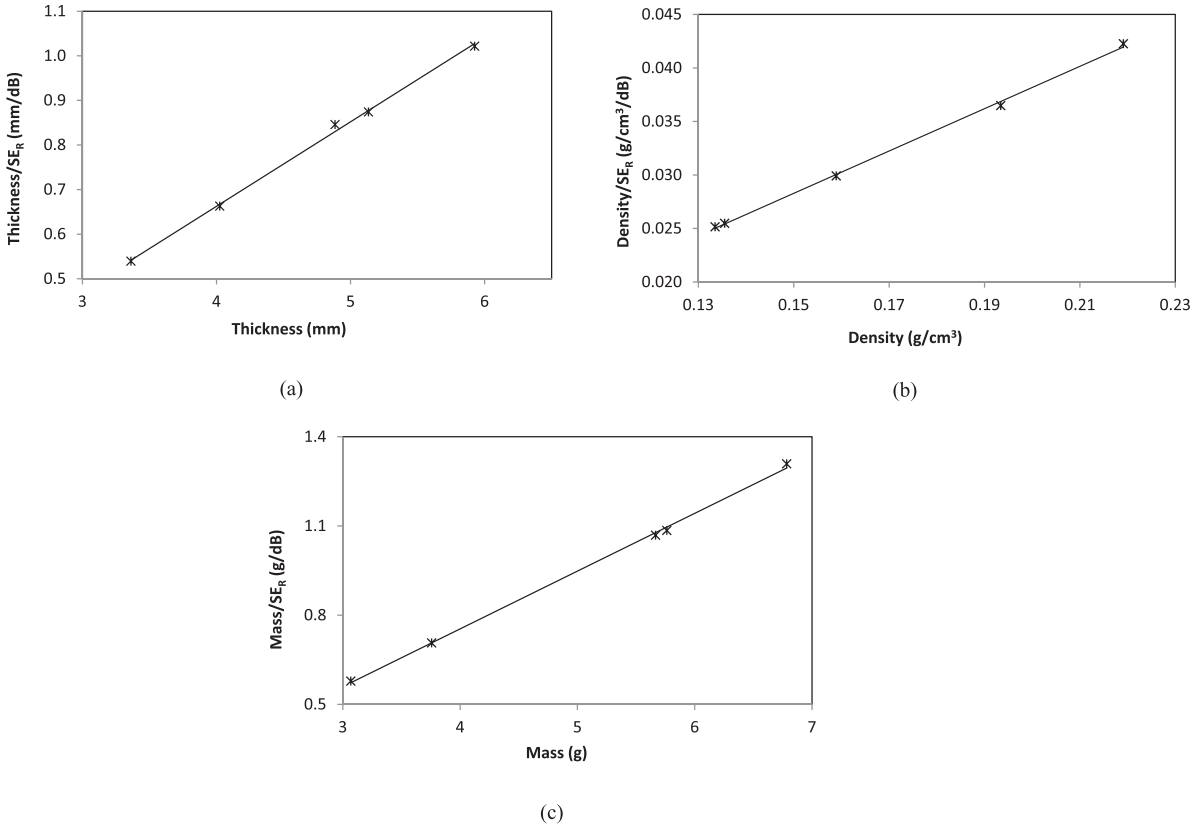

Fig. 3. Plots of (a) thickness/SE_R vs. thickness, (b) density/SE_R vs. density, and (c) mass/SE_R vs. mass. SE_R = reflection loss. Density refers to the bulk density. The curves are linear fits.

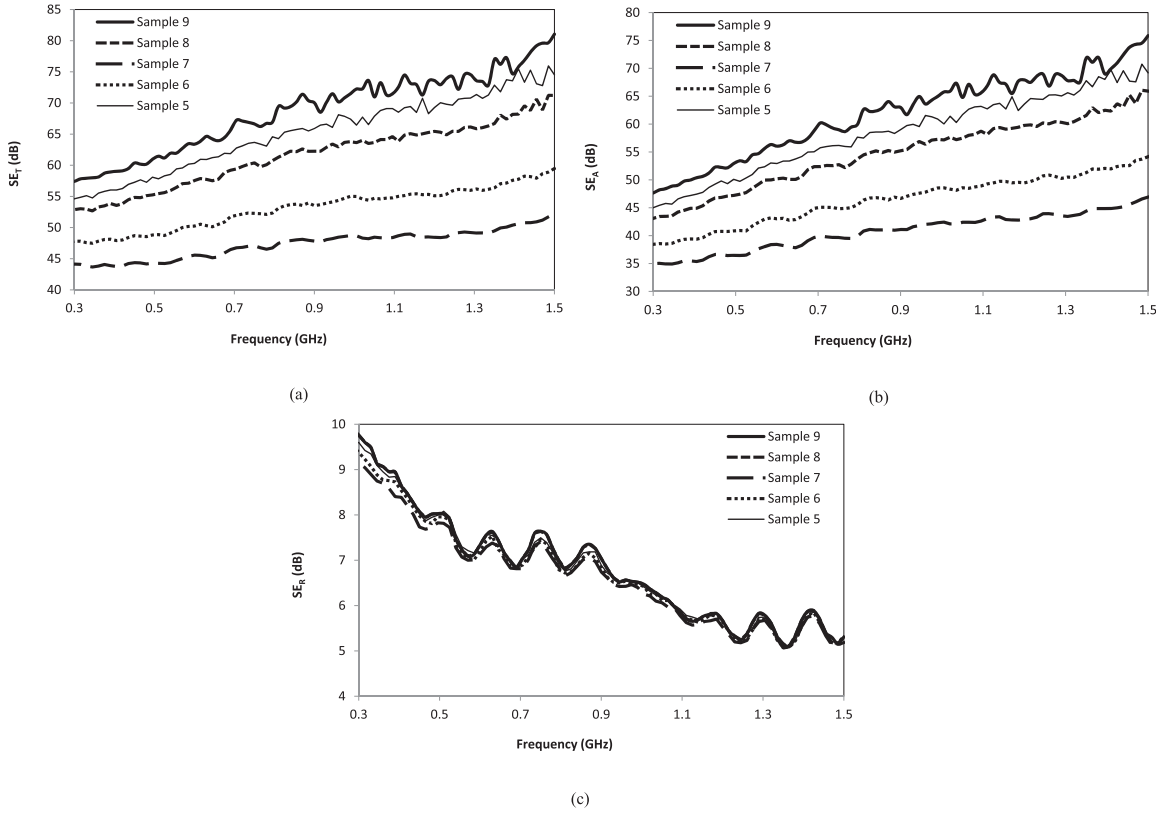

Fig. 4. The frequency dependence of (a) the shielding effectiveness (total) SE_T, (b) the absorption loss SE_A, and (c) the reflection loss SE_R, all of the CNF mats. Refer to Table 3 for the meaning of the sample numbers.

thickness and comparable shielding effectiveness per unit bulk density. The overall performance of the CNF mats is superior to that of the RGO aerogel [7], due to its higher shielding effectiveness and higher shielding effectiveness per unit thickness, though its shielding effectiveness per unit bulk density is lower. The overall performance of the CNF mats is inferior to that of CNT mats [11], graphene film [3,4] and carbon foam [2], which give very high values of the shielding effectiveness per unit thickness (1000–40000 dB/mm). The overall performance of the CNF mats is inferior to that of flexible graphite [1], which gives higher values of the shielding effectiveness (102–129 dB) and shielding effectiveness per unit thickness (42–129 dB/mm), though lower values of the shielding effectiveness per unit bulk density (93–118 dB cm^3/g).

This work shows (almost surprisingly) that the CNT mat is superior in shielding than some of the complex materials that have been recently reported for shielding. Although the CNF mat is not three-dimensionally or two-dimensionally connected (due to the absence of bonding between the adjacent CNFs), the CNF-CNF contacts in the mat are apparently good enough for the CNT mat to compete in the shielding effectiveness with graphene aerogel [5] and graphene foam [6], which are three-dimensionally connected.

4. Conclusions

The CNF mats fabricated in this work by using the paper-making method in the absence of a binder are attractive for providing relatively high values of the shielding effectiveness (52–81 dB) and the shielding effectiveness per unit bulk density (370–470 dB cm^3/g), but they provide relatively low values of the shielding effectiveness per unit thickness (14–18 dB/mm). Compared to the spun CNF mats of prior work [12,13], the CNF mats of this work exhibit higher shielding effectiveness, but lower shielding effectiveness per unit thickness. With consideration of the shielding effectiveness, shielding effectiveness per unit thickness, and shielding effectiveness per unit bulk density, the overall performance of the CNF mats is superior to that of graphene aerogel [5], RGO/PU foam [9] and RGO aerogel [7], but is inferior to that of CNT mats [11], graphene film [3,4], carbon foam [2] and flexible graphite [1]. Compared to all these carbon-containing competing materials other than flexible graphite, the CNF mats are attractive in their low fabrication cost.

Absorption is the dominant shielding mechanism of CNF mats. As a consequence, both the shielding effectiveness and the absorption loss tend to decrease with decreasing thickness. The absorption loss per unit thickness tends to decrease with increasing thickness.

The reflection loss is essentially independent of the thickness, bulk density or mass, indicating the occurrence of saturated reflection. The reflection loss per unit thickness increases with decreasing thickness, indicating that reflection mainly occurs in the surface region of the mat. The reflection loss per unit bulk density increases with decreasing bulk density, suggesting that a higher degree of three-dimensional electrical connectivity, as provided by a lower bulk density, enables reflection to occur at a greater depth into the mat surface.

The shielding effectiveness and absorption loss increase with increasing frequency, whereas the reflection loss decreases with increasing frequency. Both trends are as expected, based on electromagnetic theory.

Acknowledgement

The authors thank Ms. Asma A. Eddib of University at Buffalo, The State University of New York, for technical assistance.

References

[1] X. Luo, D.D.L. Chung, Electromagnetic interference shielding reaching 130 dB using flexible graphite, Carbon 34 (10) (1996) 1293–1294.
[2] Y. Li, B. Shen, X. Pei, Y. Zhang, D. Yi, W. Zhai, L. Zhang, Wei Xingchang, W. Zheng, Ultrathin carbon foams for effective electromagnetic interference shielding, Carbon 100 (2016) 375–385.
[3] M. Aqeeli, T. Leng, X. Huang, J.C. Chen, K.H. Chang, A. Alburaikan, Z. Hu, Electromagnetic interference shielding based on highly flexible and conductive graphene laminate, Electron. Lett. 51 (17) (2015) 1350–1352.
[4] R. Yan, K. Wang, C. Wang, H. Zhang, Y. Song, Q. Guo, J. Wang, Synthesis and in-situ functionalization of graphene films through graphite charging in aqueous $Fe_2(SO_4)_3$, Carbon 107 (2016) 379–387.
[5] W. Song, X. Guan, L. Fan, W. Cao, C. Wang, M. Cao, Tuning three-dimensional textures with graphene aerogels for ultra-light flexible graphene/texture composites of effective electromagnetic shielding, Carbon 93 (2015) 151–160.
[6] B. Shen, Y. Li, D. Yi, W. Zhai, X. Wei, W. Zheng, Microcellular graphene foam for improved broadband electromagnetic interference shielding, Carbon 102 (2016) 154–160.
[7] C. Liu, S. Ye, J. Feng, The preparation of compressible and fire-resistant sponge-supported reduced graphene oxide aerogel for electromagnetic interference shielding, Chem. - Asian J. 11 (18) (2016) 2586–2593.
[8] Z. Chen, C. Xu, C. Ma, W. Ren, H. Cheng, Lightweight and flexible graphene foam composites for high-performance electromagnetic interference shielding, Adv. Mater 25 (2013) 1296–1300.
[9] J.N. Gavgani, H. Adelnia, D. Zaarei, M. Moazzami Gudarzi, Lightweight flexible polyurethane/reduced ultralarge graphene oxide composite foams for electromagnetic interference shielding, RSC Adv. 6 (33) (2016) 27517–27527.
[10] N. Agnihotri, K. Chakrabarti, A. De, Highly efficient electromagnetic interference shielding using graphite nanoplatelet/poly(3,4-ethylenedioxythiophene)-poly(styrenesulfonate) composites with enhanced thermal conductivity, RSC Adv. 5 (54) (2015) 43765–43771.
[11] Z.P. Wu, T. Liu, D.M. Chen, G. Wu, Q.H. Wang, Y.H. Yin, Y.S. Li, Q.F. Xu, A. Krishamurthy, A facile method to improving the electromagnetic interference shielding of a free-standing and foldable carbon nanotube mat, RSC Adv. 6 (67) (2016) 62485–62490.
[12] L.D. Cremar, J. Acosta-Martinez, A. Villarreal, A. Salinas, K. Lozano, Mechanical and electrical characterization of carbon nanofibers produced from water soluble precursors, Mater. Today Commun. 7 (2016) 134–139.
[13] M. Bayat, H. Yang, F.K. Ko, D. Michelson, A. Mei, Electromagnetic interference shielding effectiveness of hybrid multifunctional Fe_3O_4/carbon nanofiber composite, Polymer 55 (3) (2014) 936–943.
[14] Hae-Rim Kim, Kazushige Fujimori, Byoung-Suhk Kim, Ick-Soo Kim, Light-weight nanofibrous EMI shielding nanowebs prepared by electrospinning and metallization, Compos. Sci. Technol. 72 (11) (2012) 1233–1239.
[15] Taejin Kim, D.D.L. Chung, Mats and fabrics for electromagnetic interference shielding, J. Mater Eng. Perf. 15 (3) (2006) 295–298.
[16] B. Wen, M. Cao, M. Lu, W. Cao, H. Shi, J. Liu, X. Wang, H. Jin, X. Fang, W. Wang, J. Yuan, Reduced graphene oxides: light-weight and high-efficiency electromagnetic interference shielding at elevated temperatures, Adv. Mater 26 (2014) 3484–3489.
[17] D.D.L. Chung, Comparison of submicron diameter carbon filaments and conventional carbon fibers as fillers in composite materials, Carbon 39 (8) (2001) 1119–1125.
[18] X. Shui, D.D.L. Chung, Submicron diameter nickel filaments and their polymer-matrix composites, J. Mater Sci. 35 (2000) 1773–1785.
[19] Y. Yang, M.C. Gupta, K.L. Dudley, R.W. Lawrence, Electromagnetic interference shielding characteristics of carbon nanofiber-polymer composites, J. Nanosci. Nanotechnol. 7 (2007) 549–554.
[20] X. Zhang, H. Pei, Z. Shen, Carbon fiber paper modified with carbon nanotube for proton exchange membrane fuel cell, Adv. Mater Res. Zuerich, Switz. 139–141 (2011) 76–79 (Pt. 1, Manufacturing Engineering and Automation I).
[21] C. Hung, C. Liu, C. Wang, W. Chen, C. Shen, H. Liang, T. Ko, Effect of conductive carbon material content and structure in carbon fiber paper made from carbon felt on the performance of a proton exchange membrane fuel cell, Renew. Energy 78 (2015) 364–373.
[22] H. Kim, Y. Lee, S. Lee, Y. Chung, Y. Yoo, Fabrication of carbon papers using polyacrylonitrile fibers as a binder, J. Mater Sci. 49 (10) (2014) 3831–3838.
[23] S. Kim, Y. Kuk, Y. Chung, F. Jin, S. Park, Preparation and characterization of polyacrylonitrile-based carbon fiber papers, J. Ind. Eng. Chem. Amst. Neth. 20 (5) (2014) 3440–3445.
[24] Z. Hu, Research on surface treatment of carbon fiber and the conductive properties of paper, Adv. Mater Res. Durnten-Zurich, Switz. 424–425 (2012) 1007–1010 (Pt. 2, Advanced Research on Engineering Materials, Energy, Management and Control).
[25] J. Song, Q. Yuan, X. Liu, D. Wang, F. Fu, W. Yang, Combination of nitrogen plasma modification and waterborne polyurethane treatment of carbon fiber paper used for electric heating of wood floors, BioResources 10 (3) (2015) 5820–5829.
[26] X. Shui, D.D.L. Chung, Electrical resistivity of submicron-diameter carbon-filament compacts, Carbon 39 (ER11) (2001) 1717–1722.
[27] C.A. Frysz, X. Shui, D.D.L. Chung, Use of carbon filaments in place of carbon black as the current collector of a lithium cell with a thionyl chloride-bromine chloride catholyte, J. Power Sources 58 (1) (1996) 55–66.

[28] Efrat Shawat, Ilana Perelshtein, Andrew Westover, Cary L. Pint, Gilbert D. Nessim, 2014 Ultra high-yield one-step synthesis of conductive and superhydrophobic three-dimensional mats of carbon nanofibers via full catalysis of unconstrained thin films, J. Mater. Chem. A 2 (36) (2014) 15118–15123.
[29] Y.J. Noh, H.S. Kim, S.Y. Kim, Carbon nanotube mat reinforced thermoplastic composites with a polymerizable, low-viscosity cyclic butylene terephthalate matrix, Macromol. Res. 22 (11) (2014) 1183–1189.
[30] M.E. Itkis, A. Pekker, X. Tian, E. Bekyarova, R.C. Haddon, Networks of semiconducting SWNTs: contribution of midgap electronic states to the electrical transport, Acc. Chem. Res. 48 (8) (2015) 2270–2279.
[31] J. Tahalyani, K.K. Rahangdale, R. Aepuru, B. Kandasubramanian, S. Datar, Dielectric investigation of a conducting fibrous nonwoven porous mat fabricated by a one-step facile electrospinning process, RSC Adv. 6 (43) (2016) 36588–36598.
[32] B. Weng, F. Xu, K. Lozano, Development of hierarchical structured carbon nanotube-nylon nanofiber mats, J. Appl. Polym. Sci. 132 (38) (2015) n/a.
[33] B. Weng, F. Xu, A. Salinas, K. Lozano, Mass production of carbon nanotube reinforced poly(methyl methacrylate) nonwoven nanofiber mats, Carbon 75 (2014) 217–226.
[34] K. Fujimori, M. Gopiraman, H. Kim, B. Kim, I. Kim, Mechanical and electromagnetic interference shielding properties of poly(vinyl alcohol)/graphene and poly(vinyl alcohol)/multi-walled carbon nanotube composite nanofiber mats and the effect of Cu top-layer coating, J. Nanosci. Nanotechnol. 13 (3) (2013) 1759–1764.
[35] A. Oroumei, H. Tavanai, M. Morshed, Radiofrequency shielding by polypyrrole-coated nano and regular fibrous mats, J. Electron. Mater 40 (11) (2011) 2256–2263.
[36] F. Nanni, C. Del Gaudio, I. Armentano, M. Dottori, A. Bianco, J.M. Kenny, G. Gusmano, Dielectric properties at microwave frequencies of poly(ε-caprolactone)/CNF films and electrospun mats, Synth. Met. 161 (9–10) (2011) 911–918.
[37] V. Bhingardive, G.P. Kar, S. Bose, Lightweight, flexible and ultra-thin sandwich architectures for screening electromagnetic radiation, RSC Adv. 6 (74) (2016) 70018–70024.
[38] D.D.L. Chung, Carbon Composites, Elsevier, 2016. Chapter 1.
[39] X. Shui, C.A. Frysz, D.D.L. Chung, Solvent cleansing of the surface of carbon filaments and its benefit to the electrochemical behavior, Carbon 33 (12) (1995) 1681–1698.
[40] X. Shui, D.D.L. Chung, High-strength high-surface-area porous carbon made from submicron-diameter carbon filaments, Carbon 34 (6) (1996) 811–814.